

Out-of-Distribution Detection with Overlap Index

Hao Fu, Prashanth Krishnamurthy, *Member, IEEE*, Siddharth Garg, *Member, IEEE*,
and Farshad Khorrani, *Senior Member, IEEE*

Abstract—Out-of-distribution (OOD) detection is crucial for the deployment of machine learning models in the open world. While existing OOD detectors are effective in identifying OOD samples that deviate significantly from in-distribution (ID) data, they often come with trade-offs. For instance, deep OOD detectors usually suffer from high computational costs, require tuning hyperparameters, and have limited interpretability, whereas traditional OOD detectors may have a low accuracy on large high-dimensional datasets. To address these limitations, we propose a novel effective OOD detection approach that employs an overlap index (OI)-based confidence score function to evaluate the likelihood of a given input belonging to the same distribution as the available ID samples. The proposed OI-based confidence score function is non-parametric, lightweight, and easy to interpret, hence providing strong flexibility and generality. Extensive empirical evaluations indicate that our OI-based OOD detector is competitive with state-of-the-art OOD detectors in terms of detection accuracy on a wide range of datasets while requiring less computation and memory costs. Lastly, we show that the proposed OI-based confidence score function inherits nice properties from OI (e.g., insensitivity to small distributional variations and robustness against Huber ϵ -contamination) and is a versatile tool for estimating OI and model accuracy in specific contexts.

Index Terms—Out-of-Distribution Detection, Overlap Index

I. INTRODUCTION

Machine learning models have been utilized in various applications [1]–[4]. However, machine learning models often struggle with out-of-distribution (OOD) samples that originate from distributions not seen during training. The OOD detection [5], [6] is a critical task to address the above issue and has been utilized in many real-world applications [6]–[9]. Given in-distribution (ID) samples originating from the training distribution, the OOD detector employs a confidence score function to quantify the distance between a given input and the available ID samples to filter out OOD inputs, thereby enhancing the machine learning model’s reliability in unseen environments.

Although numerous OOD detectors have been proposed, these approaches have a few limitations. For example, traditional OOD detectors like one-class SVM [10] are computationally and memory-efficient but are relatively less effective on large high-dimensional datasets. While deep learning approaches such as Deep SVDD [11] are capable of handling large high-dimensional datasets, they come at the cost of substantial computational and memory overhead due to their large number of parameters. Additionally, some OOD detectors (e.g., Gaussian-based OOD detectors [12]) require calculating the inverse of the covariance matrix which can be numerically

unstable. To address these limitations, this paper proposes a novel OOD detector that is non-parametric, lightweight, and effective on large high-dimensional datasets.

The proposed OOD detector employs an overlap index (OI)-based confidence score function to evaluate the likelihood of a given input belonging to the same distribution as the available ID samples. OI is a widely utilized metric that quantifies the area of intersection between two probability density functions. It is closely related to the total variation distance (TVD), where TVD is one minus OI [13]. Both OI and TVD find applications in various domains [14], [15]. Unlike Kullback–Leibler (KL) and Jensen–Shannon (JS) divergences, OI does not require the supports of the distributions to be identical and is insensitive to small distributional variations [16]. While the Wasserstein distance requires distance inference [17] and lacks robustness to Huber ϵ -contamination outliers [18] with unbounded metrics, OI does not suffer from these limitations. Despite the applications and advantages of OI, its utilization for OOD detection is seldom leveraged in existing literature. This paper endeavors to explore the potential applications of the OI-based confidence score function in OOD detection, showcasing its effectiveness.

Our OI-based confidence score function is converted from a novel upper bound of OI derived in this paper. The derived bound consists of two computationally efficient terms: the distance between the means of the clusters and the TVD between two distributions over subsets that meet specific conditions. The derived upper bound is quick to compute, non-parametric, insensitive to small distributional variations, and robust against Huber ϵ -contamination outliers. If one cluster contains only a given input and the other cluster contains a few clean ID samples, then this bound could serve as a confidence score function for evaluating the likelihood that the given input belongs to the same distribution as the available ID samples.

The proposed OI-based OOD detector addresses the aforementioned limitations of the existing OOD detectors. Compared to traditional OOD detectors, our method is empirically effective even on large high-dimensional datasets. Compared to deep OOD detectors, our OI-based detector avoids the use of neural networks, thereby being more economical in terms of computational and memory requirements. Despite this, it achieves accuracy levels comparable to those of state-of-the-art deep OOD detectors. This makes our approach particularly beneficial in scenarios where the available ID dataset is too small to effectively train a deep learning-based OOD detector. Another group of OOD detectors is Gaussian-based OOD detectors, such as GEM [12], MSP [19], Mahalanobis distance [20], and energy score [21]. These methods assume Gaussian distributions and apply distance-based metrics on deep features. Compared to them, our method neither makes distributional

The authors are with the Department of Electrical and Computer Engineering, NYU Tandon School of Engineering, Brooklyn NY, 11201. E-mail: { hf881@nyu.edu, pk929@nyu.edu, sg175@nyu.edu, khorrani@nyu.edu }

assumptions about the underlying feature space nor requires the computationally challenging and numerically unstable task of inverting covariance matrices. [22] uses an KL-based confidence scorer for OOD detection, which also assumes Gaussian distribution for the extracted features.

We show that the variant of our OI-based confidence scorer could be employed for estimating both OI and model accuracy in specific contexts. [23] estimates OI using integral probability metrics (IPM)¹, which results in a computational complexity on the order of $\mathcal{O}^*(n^\omega)$, where ω is the matrix multiplication exponent [24]. Additionally, selecting appropriate functions for IPM-based methods often presents a challenge [25]. In contrast, our method approximates OI using a class of straightforward, easily identifiable, and computationally efficient conditional functions². [13], [26] estimate OI using estimated probability density functions through kernel methods³. These methods are burdened by the curse of dimensionality [27], whereas our approach remains efficient in high-dimensional spaces.

Overall, the contributions of this paper include: 1) proposing a novel OOD detector that leverages an OI-based confidence score function; 2) evaluating the proposed OOD detector with various state-of-the-art methods and datasets to demonstrate its effectiveness and efficiency; 3) analyzing the mathematical properties of the OI-based confidence score function; and 4) exploring into the potential applications of the OI-based confidence score function for estimating OI and model accuracy in specific contexts.

The remaining part is organized as follows: We first conduct a literature review on OI and OOD detection in Sec. II. Then Sec. III derives the novel upper bound for OI and proposes our novel OI-based OOD detector. Sec. IV empirically evaluates the proposed novel OOD detector. Sec. V provides mathematical analysis and the potential applications of our approach for estimating OI and model accuracy. Sec. VI discusses the limitations and broader impact of our approach. Sec. VII concludes the paper.

II. BACKGROUND AND RELATED WORKS

A. OOD Detection

A comprehensive discussion of classic OOD detectors, such as one-class SVM [10], decision-tree [28], and one-class nearest neighbor [29], is given by [30]. The deep OOD detectors can be divided into image-level OOD detectors and feature-level OOD detectors. The image-level OOD detectors train their models using raw inputs, whereas the feature-level OOD detectors require pretrained models to process the input. For image-level OOD detectors, Deep SVDD [11], OCGAN [31], and GradCon [32] do not use additional information, whereas Deep SAD [33] uses information from anomaly samples. [34] uses a teacher network for OOD detection. CutPaste [35] considers object detection. [36] studies different autoencoders

for OOD detection. For feature-level OOD detectors, [37] achieves a higher accuracy using a transformer instead of autoencoders to reconstruct feature maps. [38] bypasses the feature reconstruction phase using self-labeled training datasets. LOE [39], Panda [40], and [41] use pretrained ImageNet models to increase their accuracy. LPIPS [42] is a feature-based similarity metric for images. ECOD [43] is a non-parametric OOD detector, which calculates the confidence score using empirical cumulative distribution functions. [44] proposes a deep isolation forest for OOD detection that uses neural networks to map original data into random representation ensembles. Other works aiming to improve OOD detection accuracy for classification and object detection include ViM [45], GradNorm [46], VOS [47], PatchCore [48], YoOOD [49]. [50] uses masked image modeling for OOD detection.

B. Statistical Divergences and Estimating OI

Popular statistical divergences to measure distribution similarities contain OI, TVD, KL divergence, and Wasserstein distance. KL divergence is often utilized in classification [51] and reinforcement learning [52], whereas the Wasserstein distance is preferred in optimal transport [53]–[56] and image processing [57]. Note that TVD is less than or equal to the square root of KL divergence. Therefore, many results from KL divergence can transfer to TVD and thus OI, or vice versa. Estimating OI and TVD with unknown distributions using only finite samples is challenging. The kernel-based estimations [13], [26] are sensitive to the choice of bandwidth, have a boundary effect, and suffer from the curse of dimensionality. We found that their methods are slow in high-dimensional space. The Cohen’s d measure [58] is efficient but assumes that the distributions A, B are Gaussian with the same standard deviation σ and approximates $OI \approx 2\Phi(-\frac{|\mu_A - \mu_B|}{2\sigma})$, where μ_A and μ_B are samples’ means and $\Phi(\cdot)$ is the standard normal distribution function. If the assumption does not hold, the method may not be accurate. [23] provides an estimator for TVD, which requires solving time-consuming linear programs and is not consistently accurate, as noted by the authors. Our OI-based confidence score function shows a potential for estimating OI in a time-efficient fashion without suffering from the curse of dimensionality.

C. Neural Network Backdoors

The neural network backdoor attack [59]–[64] has connections to data poisoning attacks [65] and adversarial attacks [66]. Some proposed backdoored triggers include Wanet [67], invisible sample-specific [68], smooth [69], and reflection [70]. Neural cleanse [71], fine-pruning [72], and [73] are backdoor defenses that require tuning model parameters. STRIP [74] needs sufficient clean samples to be accurate. NNoculation [75] and RAID [61] utilize online domain-shifted samples to improve their detectors. Our OI-based OOD detector shows effectiveness against backdoor detection using only limited clean samples without tuning any parameters or requiring online domain-shifted samples.

¹ $d_{\mathcal{F}}(P, Q) = \sup_{f \in \mathcal{F}} |\mathbb{E}X \sim P[f(X)] - \mathbb{E}Y \sim Q[f(Y)]|$, where \mathcal{F} is a class of functions.

²The condition function $\mathbb{1}\{\cdot\}$ outputs 1 when the input satisfies the given condition and 0 otherwise.

³ $\hat{f}(x) = \frac{1}{n} \sum_{i=1}^n \mathcal{K}\left(\frac{x-x_i}{\beta}\right)$, where \mathcal{K} is the kernel function and β is the bandwidth.

III. THE OI-BASED OOD DETECTOR

A. Problem Formulation and Goals

We consider the following setup. Given \mathbb{R}^n space and m samples $\{x_i\}_{i=1}^m$ that lie in an unknown distribution, we would like to build a binary detector $\Psi : \mathbb{R}^n \rightarrow \{\pm 1\}$ such that for any new input x , $\Psi(x)$ outputs 1 when x is from the same unknown probability distribution, and outputs -1, otherwise. The detector Ψ should be effective even when n is large or m is small. Additionally, the computation and memory costs of Ψ should be small.

B. The OI-Based OOD Detector

1) *Motivation: A Novel Upper Bound for OI:* Our methodology is inspired by a newly derived upper bound for the OI between bounded distributions. We consider the \mathbb{R}^n space and continuous random variables. We define P and Q as two probability distributions in \mathbb{R}^n with f_P and f_Q being their probability density functions. The derivation of this novel upper bound necessitates the introduction of the following definitions.

Definition III.1. The OI, η , is a function of two distributions whose samples belong to the \mathbb{R}^n space and outputs the overlap index value of these two distributions, which is a real number between 0 and 1. η is defined as [13]:

$$\eta(P, Q) = \int_{\mathbb{R}^n} \min[f_P(x), f_Q(x)] dx. \quad (1)$$

Definition III.2. Given an $A \subset \mathbb{R}^n$, δ_A is a function of two distributions whose samples belong to the \mathbb{R}^n space and outputs a real number between 0 and 1 with the following definition:

$$\delta_A(P, Q) = \frac{1}{2} \int_A |f_P(x) - f_Q(x)| dx. \quad (2)$$

The standard TVD is δ_A with $A = \mathbb{R}^n$ or one minus OI [13]. The following theorem shows a novel upper bound of OI between bounded distributions.

Theorem III.3. Without loss of generality, assume D^+ and D^- are two probability distributions on a bounded domain $B \subset \mathbb{R}^n$ with defined norm⁴ $\|\cdot\|$ (i.e., $\sup_{x \in B} \|x\| < +\infty$), then $\forall A \subset B$ with $A^c = B \setminus A$, we have

$$\eta \leq 1 - \frac{1}{2r_{A^c}} \|\mu_{D^+} - \mu_{D^-}\| - \frac{r_{A^c} - r_A}{r_{A^c}} \delta_A \quad (3)$$

where $r_A = \sup_{x \in A} \|x\|$ and $r_{A^c} = \sup_{x \in A^c} \|x\|$, μ_{D^+} and μ_{D^-} are the means of D^+ and D^- , and δ_A is TVD on set A as defined in **Definition III.2**. Moreover, let $r_B = \sup_{x \in B} \|x\|$, then

$$\eta \leq 1 - \frac{1}{2r_B} \|\mu_{D^+} - \mu_{D^-}\| - \frac{r_B - r_A}{r_B} \delta_A. \quad (4)$$

Since (4) holds for any A , a tighter bound can be written as

$$\eta \leq 1 - \frac{1}{2r_B} \|\mu_{D^+} - \mu_{D^-}\| - \max_A \frac{r_B - r_A}{r_B} \delta_A. \quad (5)$$

The theorem is framed to accommodate probability distributions with bounded domains. In practical applications, data

⁴This paper considers the L_2 norm. However, the analysis can be carried out using other norms.

may originate from unbounded distributions. Nevertheless, the corresponding finite-sample datasets are inherently bounded. As such, it is possible to approximate the underlying unbounded distributions with bounded ones and then apply our theorem. We forego further exploration of cases involving unbounded distributions at this time, as the current theorem sufficiently informs the intuition behind our proposed OOD detector. To calculate δ_A and $\|\mu_{D^+} - \mu_{D^-}\|$ with finite samples, we have the following corollary.

Corollary III.4. Given D^+ , D^- , B , and $\|\cdot\|$ used in **Theorem III.3**, let $A(g) = \{x \mid g(x) = 1, x \in B\}$ with any condition function $g : B \rightarrow \{0, 1\}$. An upper bound for $\eta(D^+, D^-)$ can be obtained:

$$\eta \leq \bar{\eta} = 1 - \frac{1}{2r_B} \|\mu_{D^+} - \mu_{D^-}\| - \max_g \frac{r_B - r_{A(g)}}{2r_B} |\mathbb{E}_{D^+}[g] - \mathbb{E}_{D^-}[g]|. \quad (6)$$

If we use only a single input to calculate μ_{D^+} and $\mathbb{E}_{D^+}[g]$ and use a few samples to calculate μ_{D^-} and $\mathbb{E}_{D^-}[g]$, then $\bar{\eta}$ can be considered as a confidence score function for evaluating the likelihood that the given input in D^+ belongs to the same distribution as samples in D^- . Before providing further visualization and ablation study to demonstrate the efficacy of using such a confidence score function, we present the implementation algorithm to calculate (6).

2) *Empirical Calculation of the Novel Upper Bound:* The middle term in the RHS of (6) is the distance of clusterings' means, and the last term is a function of IPM with a class of condition functions. To approximate the last term, we draw samples from D^+ and D^- and then average their g values to estimate $\mathbb{E}_{D^+}[g]$ and $\mathbb{E}_{D^-}[g]$. Alg. 1 shows the computation of $\bar{\eta}$ with given k condition functions $\{g_j\}_{j=1}^k$ and finite sample, $\{x_i^+\}_{i=1}^d \sim D^+$ and $\{x_i^-\}_{i=1}^m \sim D^-$.

Algorithm 1 ComputeBound($\{x_i^+\}_{i=1}^d, \{x_i^-\}_{i=1}^m, \{g_j\}_{j=1}^k$)

```

 $B \leftarrow \{x_1^+, \dots, x_d^+, x_1^-, \dots, x_m^-\}$ 
 $r_B \leftarrow \max_{x \in B} \|x\|$ 
 $\Delta_\mu \leftarrow \left\| \frac{1}{d} \sum_{i=1}^d x_i^+ - \frac{1}{m} \sum_{i=1}^m x_i^- \right\|$ 
for  $j = 1 \rightarrow k$  do
   $A(g_j) \leftarrow \{x \mid g_j(x) = 1, x \in B\}$ 
   $r_A \leftarrow \max_{x \in A} \|x\|$ 
   $s_j \leftarrow (r_B - r_A) \left| \frac{1}{d} \sum_{i=1}^d g_j(x_i^+) - \frac{1}{m} \sum_{i=1}^m g_j(x_i^-) \right|$ 
end for
Return:  $1 - \frac{1}{2r_B} \Delta_\mu - \frac{1}{2r_B} \max_j s_j$ 

```

Choice of g : The choice of condition functions is not unique. The literature faces similar issues when choosing functions for IPMs [23], [25]. The overall guideline is to choose functions that satisfy convenient regularity conditions. The chosen functions should also be computation-efficient and memory-efficient. Considering all the aspects, $g_j(x) = \mathbb{1}\{r_{j-1} \leq \|x\| \leq r_j\}$ is selected with $r_j = jr_B/k$, which are nicely regularized, computation-efficient, and empirically effective. However, other condition functions are worth exploring.

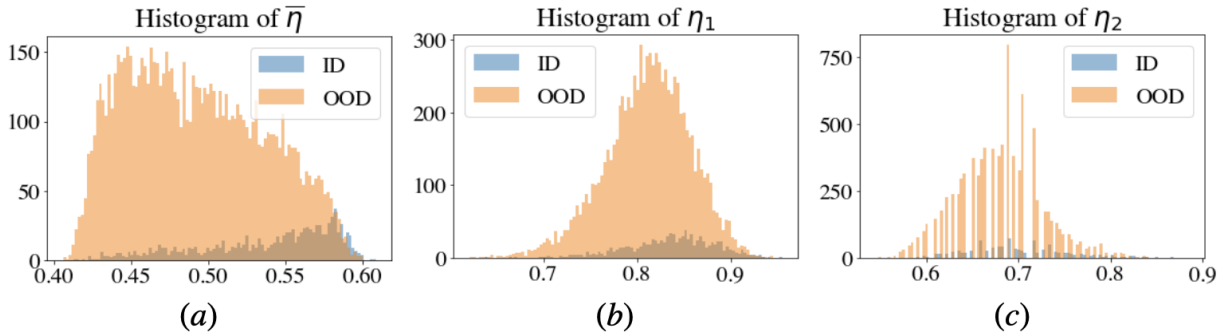


Fig. 1. Histograms of confidence scores using $\bar{\eta}$, η_1 , and η_2 with plane as the ID class and the other nine classes as the OOD class in CIFAR-10.

3) *The OI-Based Confidence Score Function:* The confidence score function using Alg. 1 is defined as $f(x) = \text{ComputeBound}(\{x\}, \{x_i\}_{i=1}^m, \{g_j\}_{j=1}^k)$ (i.e., $\{x^+\}^d = \{x\}$ with $d = 1$), which measures the maximum similarity between x and $\{x_i\}_{i=1}^m$. If $f(x) \geq T_0$, then x is considered as an ID sample. Otherwise, x is considered as an OOD sample. T_0 is pre-defined by the user.

C. Discussion of the OI-Based OOD Detector

1) *Computation and Space Complexities:* We can pre-compute and store $\frac{1}{m} \sum_{i=1}^m x_i$ and $\frac{1}{m} \sum_{i=1}^m g_j(x_i)$ in Alg. 1. Therefore, the space complexity is $\mathcal{O}(k + 1)$. The computation complexity is $\mathcal{O}(k + 1)$ for each online input x since it needs to calculate $\|x\|$ once and s_j for k times. k can be restricted to a reasonable number (e.g., ≤ 100) so that even devices without strong computation power (e.g., Arduino or Raspberry Pi) can run our OOD detector efficiently. This is an advantage compared to time-consuming deep approaches.

2) *Visualization:* Although our confidence score seems simple, we empirically find it effective. Both $\frac{1}{2r_B} \|\mu_{D^+} - \mu_{D^-}\|$ and $\max_g \frac{r_B - r_A(g)}{2r_B} |\mathbb{E}_{D^+}[g] - \mathbb{E}_{D^-}[g]|$ are important for our OOD detector. To validate their efficacy, we created two another OOD detectors with $\eta_1 = 1 - \frac{1}{2r_B} \|\mu_{D^+} - \mu_{D^-}\|$ and $\eta_2 = 1 - \max_g \frac{r_B - r_A(g)}{2r_B} |\mathbb{E}_{D^+}[g] - \mathbb{E}_{D^-}[g]|$ as the confidence score functions. Fig. 1 shows the histograms of η , η_1 , and η_2 using CIFAR-10 [76] plane images as the ID samples and the other nine class images as the OOD samples. Fig. 1(b,c) show that it is less likely to distinguish between ID and OOD samples by independently observing either $\frac{1}{2r_B} \|\mu_{D^+} - \mu_{D^-}\|$ or $\max_g \frac{r_B - r_A(g)}{2r_B} |\mathbb{E}_{D^+}[g] - \mathbb{E}_{D^-}[g]|$. However, the summation of $\frac{1}{2r_B} \|\mu_{D^+} - \mu_{D^-}\|$ and $\max_g \frac{r_B - r_A(g)}{2r_B} |\mathbb{E}_{D^+}[g] - \mathbb{E}_{D^-}[g]|$ amplifies the difference between ID and OOD samples, as shown in Fig. 1(a). Our OOD detector successfully utilizes the dependence between $\frac{1}{2r_B} \|\mu_{D^+} - \mu_{D^-}\|$ and $\max_g \frac{r_B - r_A(g)}{2r_B} |\mathbb{E}_{D^+}[g] - \mathbb{E}_{D^-}[g]|$ to identify OOD samples.

3) *Flexibility:* Our OOD detector does not require any distributional assumptions nor the need to calculate the inverse of the covariance matrix which can be numerically unstable. Besides, Alg. 1 could be applied in any space, such as the feature space generated by a pretrained model. This flexibility broadens the potential application of our approach. Additionally,

TABLE I
INFORMATION ON UTILIZED UCI DATASETS.

| Dataset | n | ID Class | Size | OOD Class | Size |
|---------------|-----|--------------|------|-------------|------|
| Iris | 4 | Setosa | 50 | Vers.+Virg. | 100 |
| | | Versicolour | 50 | Seto.+Virg. | 100 |
| | | Virginica | 50 | Seto.+Vers. | 100 |
| Breast Cancer | 9 | Malignant | 241 | Beni. | 458 |
| | | Benign | 458 | Mali. | 241 |
| Ecoli | 7 | Peripalsm | 52 | All Others | 284 |
| Ball-bearing | 32 | Ball-bearing | 913 | None | 0 |

TABLE II
INFORMATION ON UTILIZED DATASETS.

| Dataset | Dimension | # Class | # Training | # Testing |
|--------------|---------------------------|---------|------------|-----------|
| CIFAR-10 | $3 \times 32 \times 32$ | 10 | 50000 | 10000 |
| CIFAR-100 | $3 \times 32 \times 32$ | 100 | 50000 | 10000 |
| Textures | $3 \times 32 \times 32$ | 47 | N/A | 5640 |
| SVHN | $3 \times 32 \times 32$ | 10 | N/A | 26032 |
| LSUN_C | $3 \times 36 \times 36$ | 1 | N/A | 10000 |
| LSUN_R | $3 \times 32 \times 32$ | 1 | N/A | 10000 |
| iSUN | $3 \times 32 \times 32$ | 1 | N/A | 8925 |
| MNIST | $1 \times 28 \times 28$ | 10 | 60000 | 10000 |
| GTSRB | $3 \times 32 \times 32$ | 43 | 39209 | 12630 |
| YouTube Face | $3 \times 55 \times 47$ | 1283 | 103923 | 12830 |
| sub-ImageNet | $3 \times 224 \times 224$ | 200 | 100000 | 2000 |

Alg. 1 supports batch-wise computation since $\frac{1}{m} \sum_{i=1}^m x_i$ and $\frac{1}{m} \sum_{i=1}^m g_j(x_i)$ can be pre-computed and stored.

IV. EXPERIMENTAL RESULTS

A. Setup

Datasets: We employ UCI datasets [77] for benchmarking against traditional OOD detectors. Table I provides detailed information about the selected UCI datasets. For comparison with state-of-the-art deep OOD detectors, we primarily use the CIFAR-10 dataset [76] in both input and feature spaces. Additionally, the CIFAR-100 dataset [76] is utilized to serve as the ID dataset for comparisons with Gaussian-based OOD detectors. OOD datasets include Textures [78], SVHN [79], LSUN-Crop [80], LSUN-Resize [80], and iSUN [81]. We also extend the application of our OOD detector to backdoor detection, leveraging datasets such as MNIST [82], GTSRB [83], YouTube Face [84], and sub-ImageNet [85]. Details on these datasets are provided in Table II.

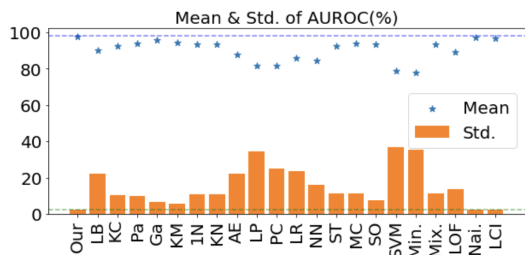


Fig. 2. AUROC on UCI datasets. Horizontal dashed lines: the mean and standard deviation of our approach.

Metrics: The primary metric employed for assessing the efficacy of our OOD detectors is the area under the receiver operating characteristic curve (AUROC). A higher AUROC value indicates better accuracy in differentiating between ID and OOD samples. Supplementary to AUROC, we also utilize TPR95—representing the detection accuracy for OOD samples when the detection accuracy for ID samples is fixed at 95%—and the area under the precision-recall curve (AUPR) as additional performance metrics.

Hyperparameters of our OOD detector: We set $k = 100$ and $g_j(x)$ with the form $\mathbb{1}\{r_{j-1} \leq \|x\| \leq r_j\}$ in Alg. 1. We recommend choosing k between 50 and 200. Values of $k \geq 200$ do not significantly improve performance, while $k < 50$ results in underperformance. The selected condition functions g_j are both computationally efficient and empirically effective. The number m of available ID samples varies depending on the dataset in use. We perform ablation studies to evaluate the impact of these hyperparameters on our method’s performance.

Hyperparameters of compared methods: We obtained the code for each comparison method from the authors’ respective websites. The hyperparameters were carefully fine-tuned to replicate the results reported in their original papers. For instances where we applied the compared methods to new datasets, we conducted careful hyperparameter tuning to ensure their best performance.

B. Comparison Results

UCI Dataset: We first evaluated our OI-based detector on small UCI datasets given in Table I. Fig. 2(a) shows that our detector outperforms all baseline methods by showing the highest average AUROC (i.e., $97.67 \pm 2.55\%$). Table X in the appendix provides the numerical numbers.

CIFAR-10 Dataset: We then use CIFAR-10 images with one class being ID and the remaining classes being OOD. The compared deep OOD detectors on raw images without using additional information from anomaly samples include DCAE [86], AnoGAN [87], Deep SVDD [11], OCGAN [31], and GradCon [32]. Comparisons with more recent approaches are provided later. All the methods are given $m = 5000$ available ID samples. The result is in Table III “Raw Image Space”. Our approach shows the highest AUROC. Although the baseline methods could reach similar accuracy, they are slower than ours on the same CPU machine. For example, the Deep SVDD requires 446.8 ms for each detection (ours is 3 ms). Fig. 3(a) shows the AUROC of our approach with m less than 5000.

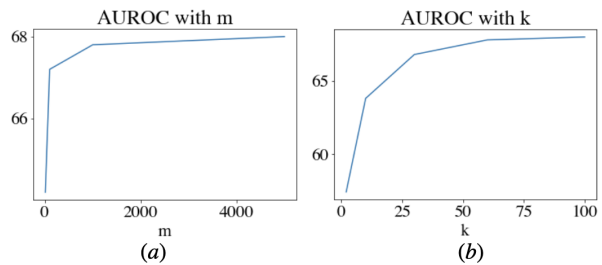


Fig. 3. AUROC of our approach with (a) different numbers m of available ID samples and (b) different numbers k of condition functions.

With only $m = 100$ ID samples, the AUROC of our approach is 67.2%. In contrast, the AUROC of Deep SVDD drops to 61.1% with $m = 100$. As for the memory cost, Deep SVDD uses LeNet [88] with three convolutional layers. The first layer already has 2400 parameters, whereas our approach has $\mathcal{O}(k + 1)$ space complexity with $k = 100$.

Ablation Study: We compare our approach with classic OOD detectors that are fit by samples’ norms, including LOF [89], OCSVM [10], Isolation Forest [90], and Elliptic Envelope [91]. Table IV shows that our approach is more than just calculating the statistic of the sample’s norms. When using η_1 and η_2 mentioned in Sec. III as the confidence score functions, the AUROC of our approach becomes 58.4% for η_1 and 50.1% for η_2 . These two numbers are consistent with Fig. 1 that either term cannot individually detect OOD samples. Fig. 3(b) shows the AUROC of our approach with different k . Our approach remains high AUROC when $k \geq 50$.

Runtime Efficiency: ECOD [43] is also non-parametric and does not require training parameters. The time complexity of ECOD is $\mathcal{O}(n)$ that increases with the data dimension n . We compare the execution time of our approach with ECOD by varying the data dimension n . We also report the computation time of Deep Isolation Forest [44]. Table V shows the execution time. The computation complexity of our method and Deep Isolation Forest do not increase with the data dimension, whereas the computation complexity of ECOD increases linearly with the data dimension. The time complexity of our approach increases linearly with the number k of utilized condition functions. We empirically observed that with $k = 1000$, the execution time becomes 36 ms.

Improvement with Extra Information: Deep OOD detectors such as LPIPS [42], Bergmann’s method [34], Panda [40], and ADTR [37] require pretrained models or additional information from anomaly samples to identify OOD samples. If our approach is also allowed to use pretrained models and information from anomaly samples, the accuracy will improve. Specifically, we use a pretrained ImageNet model from [40] to extract CIFAR-10 features. We also assume that a contaminated dataset is available. To build the contaminated dataset, we first merge all ID and OOD samples and then randomly select 100 samples. During the testing, each input will be subtracted from the mean vector of this contaminated dataset. The results are shown in Table III “Extra Information”. The average AUROC of our approach increases to 96.2%. Fig. 4(a) shows the improvement of our approach. According to Fig. 4(b),

TABLE III
AUROC (%) ON CIFAR-10 WITH EACH CLASS BEING ID. **Boldface** SHOWS THE HIGHEST AUROC.

| Class | Raw Image Space | | | | | | Extra Information | | | | |
|-------|-----------------|-------------|-------------|--------|------|-------------|-------------------|-------|---------|-------|-------------|
| | Ours | OCgan | Deep SVDD | AnoGAN | DCAE | GradCon | Ours | LPIPS | Bergman | PANDA | ADTR |
| Plane | 76.7 | 75.7 | 61.7 | 67.1 | 59.1 | 76.0 | 96.1 | 79.3 | 78.9 | 93.9 | 96.2 |
| Car | 67.0 | 53.1 | 65.9 | 54.7 | 57.4 | 59.8 | 97.5 | 94.6 | 84.9 | 97.1 | 98 |
| Bird | 53.4 | 64.0 | 50.8 | 52.9 | 48.9 | 64.8 | 94 | 63.1 | 73.4 | 85.4 | 94.5 |
| Cat | 58.5 | 62.0 | 59.1 | 54.5 | 58.4 | 58.6 | 94.3 | 73.7 | 74.8 | 85.4 | 91.7 |
| Deer | 73.0 | 72.3 | 60.9 | 65.1 | 54.0 | 73.3 | 95.7 | 72 | 85.1 | 93.6 | 95.1 |
| Dog | 66.2 | 62.0 | 65.7 | 60.3 | 62.2 | 60.3 | 96.4 | 75.2 | 79.3 | 91.2 | 95.6 |
| Frog | 73.3 | 72.3 | 67.7 | 58.5 | 51.2 | 68.4 | 97.9 | 83.6 | 89.2 | 94.3 | 98 |
| Horse | 58.8 | 57.5 | 67.3 | 62.5 | 58.6 | 56.7 | 94.9 | 81.8 | 83 | 93.5 | 97.1 |
| Ship | 78.0 | 82.0 | 75.9 | 75.8 | 76.8 | 78.4 | 97.9 | 81.2 | 86.2 | 95.1 | 98 |
| Truck | 74.7 | 55.4 | 73.1 | 66.5 | 67.3 | 67.8 | 97.1 | 86.3 | 84.8 | 95.2 | 96.9 |
| Ave. | 68.0 | 65.6 | 64.8 | 61.8 | 59.4 | 66.4 | 96.2 | 79.1 | 82.0 | 92.5 | 96.1 |

TABLE IV
AUROC OF OUR APPROACH USING η_1 AND η_2 AS THE CONFIDENCE SCORE FUNCTIONS AND AUROC OF OTHER METHODS WITH SAMPLES' NORMS AS INPUTS.

| Method | η_1 | η_2 | LOF | OCSVM | Ellip. Env. | Iso. Fo |
|--------|----------|----------|------|-------|-------------|---------|
| AUROC | 58.4 | 50.1 | 60.5 | 55.2 | 55.2 | 56.7 |

TABLE V
EXECUTION TIME (MS) PER SAMPLE WITH VARIOUS DATA DIMENSION.

| n | 10 | 100 | 500 | 1000 | 2000 |
|-----------------------|-----|-----|-----|------|------|
| Ours | 3 | 3 | 3 | 3 | 3 |
| ECOD | 8 | 79 | 453 | 1021 | 2245 |
| Deep Isolation Forest | 150 | 150 | 150 | 150 | 150 |

$\max_g \frac{r_B - r_{A(g)}}{2r_B} |\mathbb{E}_{D^+}[g] - \mathbb{E}_{D^-}[g]|$ helps distinguish between ID samples and OOD samples after using the pretrained model and the contaminated dataset. Although the compared methods may show similar performance, their training time (e.g., PANDA) is much higher than ours.

Large-Scale Datasets: We evaluated our approach on large-scale datasets following a similar procedure. Specifically, we used the pretrained model CLIP [92] as the feature extractor, with ImageNet-1K [46] as the ID dataset and iNaturalist [93], SUN [94], Textures [78], and Places [95] as the OOD datasets. The extracted text embeddings of ImageNet-1K labels served as the ID features for our OI-based detector. The utilized prompt is "the < >" with the blank filled by specific labels. For example, if the class is cat, then the generated prompt would be "the cat". During inference, for a given image, we extracted its image embedding using CLIP and calculated the OI value between this embedding and the text embeddings of

ID labels. To build the contaminated dataset, we merged all ID and OOD features, then randomly selected 100 features. During testing, each feature was subtracted from the mean vector of this contaminated dataset. The compared methods are allowed to use ImageNet-1K training data to train or fine-tune their OOD detectors. The results, shown in Table VIII, demonstrate consistent performance of our approach on large-scale datasets.

Gaussian-Based Approaches: We feed raw data into WideResNet pretrained models to extract complex high-dimensional features whose shape is $128 \times 8 \times 8$. The pretrained models are downloaded from [12]. The compared methods are MSP [19], Mahalanobis [20], Energy score [21], GEM [12], and VOS [47]. All baseline methods are evaluated in the same feature space with their optimal hyperparameters for fair comparisons. We formed a small dataset by randomly selecting ten samples from each class to form the available ID dataset. Table VI shows the experimental results of our approach compared with Gaussian-based approaches for the feature-level OOD detection when CIFAR-10 and CIFAR-100 are the ID datasets and Textures, SVHN, LSUN-Crop, LSUN-Resize, and iSUN are the OOD datasets. Table VII shows the computation time and memory cost of our approach and the other methods. Our approach outperforms the other methods using the least memory, showing the highest TPR95 and AUROC on average. The AUPR of our approach is in the same range as other baseline methods. We further evaluated our approach using different numbers k of conditions functions and plotted the results in Fig. 5. From the figure, the performance of our approach increases with k and eventually converges, which is consistent with Fig. 3(b).

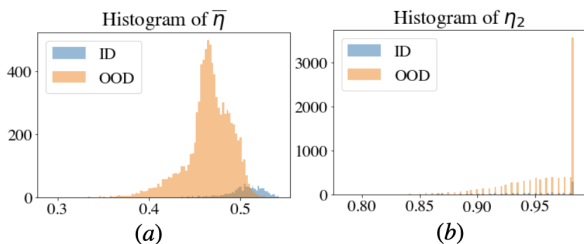


Fig. 4. Histograms of confidence scores using $\bar{\eta}$ and η_2 with plane as the ID class and the other nine classes as the OOD class in CIFAR-10.

Backdoor Detection: We applied our approach to backdoor detection [59] by considering clean samples as ID data and poisoned samples as OOD data. We created different backdoored models and used them to extract data features. We compare with previous baseline methods plus STRIP [74]. The average performance is given in Table IX. Our approach detects various attacks [61], [67], [68], [98], [99] and outperforms other baseline methods by showing the highest average AUROC. Details are provided in Appendix G.

TABLE VI

RESULTS FOR CIFAR-10 AND CIFAR-100 BEING IN-DISTRIBUTION DATASETS. **Boldface** SHOWS THE BEST PERFORMANCE, WHEREAS UNDERLINE SHOWS THE SECOND BEST.

| Out-of-Distribution Datasets | Method | ID Dataset: CIFAR-10 | | | ID Dataset: CIFAR-100 | | |
|------------------------------|--------------|----------------------|--------------|--------------|-----------------------|--------------|--------------|
| | | TPR95 (%) | AUROC (%) | AUPR (%) | TPR95 (%) | AUROC (%) | AUPR (%) |
| Texture | Ours | <u>64.20</u> | 92.80 | 92.33 | 42.50 | 85.79 | 85.27 |
| | MSP | 40.75 | 88.31 | 97.08 | 16.71 | 73.58 | 93.02 |
| | Mahalanobis | 62.38 | <u>94.46</u> | <u>98.75</u> | <u>57.62</u> | <u>90.14</u> | 97.62 |
| | Energy Score | 47.47 | 85.47 | 95.58 | 20.38 | 76.46 | 93.68 |
| | GEM | 72.61 | 94.59 | 98.79 | 57.40 | 90.17 | <u>97.63</u> |
| | VOS | 53.55 | 86.81 | 95.72 | 59.08 | 88.05 | 97.99 |
| SVHN | Ours | 94.10 | 98.56 | 99.41 | 93.75 | 98.36 | 99.36 |
| | MSP | 52.41 | 92.11 | 98.32 | 15.66 | 71.37 | 92.89 |
| | Mahalanobis | <u>79.34</u> | <u>95.72</u> | <u>99.04</u> | 51.35 | 89.25 | 97.52 |
| | Energy Score | 64.20 | 91.05 | 97.66 | 14.59 | 74.10 | 93.65 |
| | GEM | 79 | 95.65 | 99.01 | 51.51 | <u>89.40</u> | <u>97.57</u> |
| | VOS | 75.41 | 95.26 | 98.99 | <u>51.66</u> | 87.13 | 96.85 |
| LSUN-Crop | Ours | 83.63 | 96.60 | 96.61 | 57.76 | 89.95 | 90.03 |
| | MSP | 69.07 | 95.64 | 99.13 | 33.44 | 83.71 | 96.32 |
| | Mahalanobis | 30.06 | 86.15 | 97.05 | 1.53 | 58.48 | 89.73 |
| | Energy Score | <u>91.89</u> | <u>98.40</u> | 99.67 | <u>64.01</u> | <u>93.41</u> | <u>98.59</u> |
| | GEM | 30.20 | <u>86.09</u> | 97.03 | 1.70 | 58.42 | 89.70 |
| | VOS | 92.45 | 98.44 | 99.67 | 91.94 | 98.38 | 99.65 |
| LSUN-Resize | Ours | <u>85.41</u> | <u>96.84</u> | 96.86 | 88.49 | 97.56 | 97.55 |
| | MSP | 47.45 | 91.30 | 98.11 | 16.54 | 75.32 | 94.03 |
| | Mahalanobis | 35.64 | 88.12 | 97.45 | <u>67.20</u> | 93.97 | 98.70 |
| | Energy Score | 71.75 | 94.12 | <u>98.64</u> | 21.38 | 79.29 | 94.97 |
| | GEM | 35.45 | 88.09 | 97.43 | 67.09 | 94.01 | 98.70 |
| | VOS | 85.85 | 97.19 | 99.41 | 63.91 | 90.95 | 97.74 |
| iSUN | Ours | <u>79.62</u> | <u>95.64</u> | 95.68 | 82.15 | 96.05 | 96.24 |
| | MSP | 43.40 | 89.72 | 97.72 | 17.02 | 75.87 | 94.20 |
| | Mahalanobis | 26.77 | 87.87 | 97.33 | 64.07 | 92.69 | 98.32 |
| | Energy Score | 66.27 | 92.56 | <u>98.25</u> | 19.20 | 78.98 | 94.90 |
| | GEM | 36.80 | 87.85 | 93.33 | <u>64.10</u> | <u>92.73</u> | 98.32 |
| | VOS | 82.29 | 96.53 | 99.25 | 63.01 | 90.91 | 97.95 |
| Average Performance | Ours | 81.39 | 96.08 | 96.17 | 72.93 | 93.53 | 93.69 |
| | MSP | 50.63 | 91.46 | <u>98.07</u> | 19.87 | 75.97 | 94.09 |
| | Mahalanobis | 46.83 | 90.46 | 97.92 | 48.35 | 84.90 | 96.37 |
| | Energy Score | 68.31 | 92.32 | 97.96 | 27.91 | 80.44 | 95.15 |
| | GEM | 50.81 | 90.45 | 97.91 | 48.36 | 84.94 | <u>96.38</u> |
| | VOS | <u>77.91</u> | <u>94.84</u> | 98.60 | <u>65.92</u> | <u>91.08</u> | 98.03 |

TABLE VII

COMPARISON IN COMPUTATION TIME AND MEMORY COST DURING INFERENCE.

| ID | Method | Time/Sample | Memory |
|-----------|---------|---------------|-------------------|
| CIFAR-10 | Ours | 3.0ms | 1048.22MiB |
| | MSP | 0.02ms | 1825.21MiB |
| | Mahala. | 30.61ms | 1983.17MiB |
| | Energy | 0.22ms | 1830.01MiB |
| | GEM | 25.62ms | 1983.51MiB |
| | VOS | 19.56ms | 1984.05MiB |
| CIFAR-100 | Ours | 3.0ms | 1134.32MiB |
| | MSP | 0.02ms | 1825.98MiB |
| | Mahala. | 56.24ms | 1983.81MiB |
| | Energy | 0.21ms | 1838.23MiB |
| | GEM | 56.27ms | 1984.77MiB |
| | VOS | 20.32ms | 1984.91MiB |

TABLE VIII

AUROC OF OUR APPROACH ON LARGE-SCALE DATASETS. THE ID DATASET IS IMAGENET-1K. THE BACKBONE IS ViT-B/16.

| OOD Datasets | iNaturalist | SUN | Places | Textures | Ave. |
|---------------|--------------|--------------|--------------|--------------|---------------|
| MSP [19] | 87.44 | 79.73 | 79.67 | 79.69 | 81.633 |
| ODIN [96] | 94.65 | 87.17 | 85.54 | 87.85 | 88.803 |
| GradNorm [46] | 72.56 | 72.86 | 73.70 | 70.26 | 72.345 |
| ViM [45] | 93.16 | 87.19 | 83.75 | 87.18 | 87.820 |
| KNN | 94.52 | 92.67 | 91.02 | 85.67 | 90.970 |
| VOS [47] | 94.62 | 92.57 | 91.23 | 86.33 | 91.188 |
| NPOS [97] | 96.19 | 90.44 | 89.44 | 88.80 | 91.218 |
| Ours | 99.57 | 92.78 | 88.31 | 94.92 | 93.895 |

TABLE IX

AVERAGE PERFORMANCE OF DIFFERENT OOD DETECTORS FOR BACKDOOR DETECTION.

| Metrics (%) | Ours | STRIP | Mahalanobis | GEM | MSP |
|-------------|--------------|-------|-------------|--------------|-------|
| TPR95 | 89.40 | 39.60 | 56.97 | 91.57 | 39.24 |
| AUROC | 96.68 | 70.30 | 75.94 | 58.08 | 54.92 |
| AUPR | 95.42 | 68.76 | 76.37 | 75.88 | 60.52 |

V. ANALYSIS

A. Mathematical Properties

Proposition V.1. Consider uniform distribution for D^+ in $[0, 1]$ and $1 + \sin 2\pi\omega x$ for D^- in $[0, 1]$, with $g(x) = \mathbb{1}\{|x| \leq r\}$, the proposed confidence score function $\bar{\eta}$ is insensitive to small distribution variations:

$$\bar{\eta}(D^+, D^-) \geq 1 - \frac{1}{\omega} \quad \forall \omega \geq 1. \quad (7)$$

Proposition V.2. Let $\epsilon \in [0, 1]$, then for arbitrary D^+ , D^- , and g , the proposed confidence score function $\bar{\eta}$ is robust against Huber- ϵ contamination:

$$\bar{\eta}(D^+, (1 - \epsilon)D^+ + \epsilon D^-) \geq 1 - \epsilon. \quad (8)$$

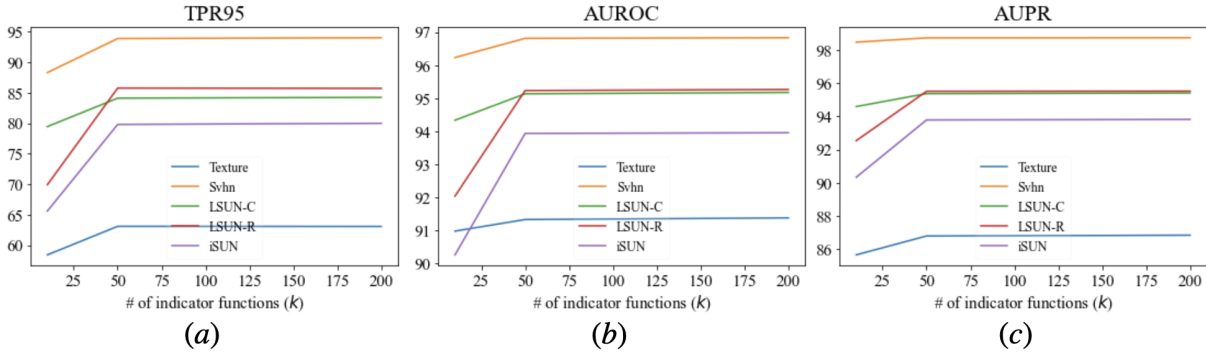


Fig. 5. Performance of our approach with different numbers ($k = 10, 50, 200$) of condition functions for CIFAR-10 being ID data.

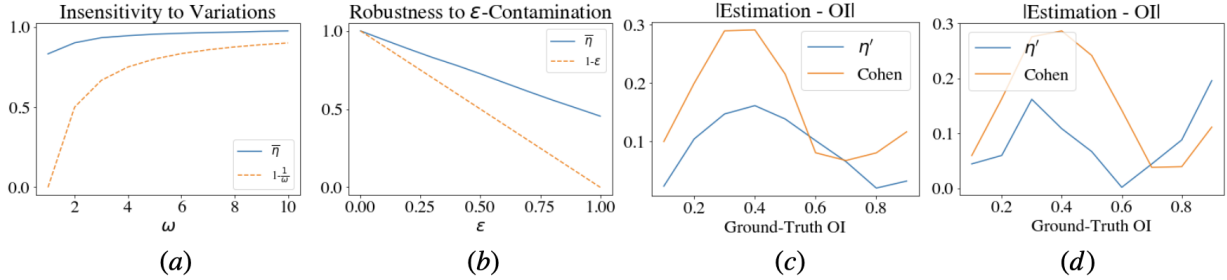


Fig. 6. (a): illustration of **Proposition V.1**. (b): illustration of **Proposition V.2**. (c,d): the absolute value of estimation errors between the ground-truth OI and $\bar{\eta}'$ for uniform distributions (c) and truncated Gaussian distributions (d).

The insensitivity and robustness are illustrated in Fig. 6(a,b). The following theorem shows the potential of our OI-based confidence score function for estimating the model accuracy.

Theorem V.3. Assume that D and D^* are two different data distributions with $\eta(D, D^*) < 1$ and denote the overall accuracy of the model on D^* as Acc . If a model has a training accuracy p on D and a testing accuracy q on $D^* \setminus D$, then we have

$$Acc \leq (p - q) \left(1 - \frac{1}{2r_B} \|\mu_D - \mu_{D^*}\|\right) - \max_g \frac{r_B - r_{A(g)}}{2r_B} |\mathbb{E}_D[g] - \mathbb{E}_{D^*}[g]| + q. \quad (9)$$

Theorem V.3 provides a theoretical interest for OOD generalization and is also empirically useful when the domain shift happens in the backdoor setting, where the model has zero clean accuracy on poisoned data (i.e., $q = 0$). Define the clean distribution as D , poisoned distribution as D^p , and a testing distribution D^* with $D^* = \sigma D + (1 - \sigma)D^p$, where $\sigma \in [0, 1]$. Then (9) becomes

$$Acc \leq p \left(1 - \frac{1 - \sigma}{2r_B} \|\mu_D - \mu_{D^p}\|\right) - (1 - \sigma) \max_g \frac{r_B - r_{A(g)}}{2r_B} |\mathbb{E}_D[g] - \mathbb{E}_{D^p}[g]|. \quad (10)$$

The experimental illustration is given in Appendix H.

B. OI Estimation

Let $\bar{\eta}' = \max\{0, 1 - \max_g \frac{r_B - r_{A(g)}}{2r'} |\mathbb{E}_{D^+}[g] - \mathbb{E}_{D^-}[g]| - \frac{1}{2r'} \|\mu_{D^+} - \mu_{D^-}\|\}$ be the variant of $\bar{\eta}$ given in (6), where

$r' \leq r_B$. For any given r' , we could use Alg. 1 to calculate $\bar{\eta}'$ as an estimate of OI. To validate $\bar{\eta}'$, we consider estimate OI in \mathbb{R}^4 . We set r' as the median Euclidean norm among all vectors in B , use indicator functions $g_j(x) = \mathbb{1}\{\|x\| \leq r_j\}$, and choose $k = 100$ and $m = 50$. The utilization distributions are truncated Gaussian and uniform. We merged the two data clusterings and computed the mean vector of the combined set. We set this mean vector as the origin. The results are illustrated in Fig. 6(c,d). We empirically observed that the computation and memory costs of using the kernel estimator [13] in \mathbb{R}^4 are much higher than ours and Cohen's d measure [58]. Therefore, we only show the comparison results with Cohen's d measure. The findings suggest that our OI-based confidence score function shows promise for applications in OI estimation.

VI. LIMITATION AND BROADER IMPACT

[100] proves that for any OOD detector, there exist situations where the OOD samples lie in the high probability or density regions of ID samples, and the OOD method performs no better than the random guess. We empirically observed that by shifting in- and out-distribution clusterings to the origin, our approach becomes less effective, supporting [100]'s claim. Due to this limitation, the attacker may use our work to design stealthy OOD samples to evade our detection, causing machine learning systems to malfunction. Nevertheless, we believe that the positive impact of our approach far outweighs any potential negative societal impact.

VII. CONCLUSION

This paper proposes a novel OOD detection approach that strikes a favorable balance between accuracy and computational efficiency. The utilized OI-based confidence score function is non-parametric, computationally lightweight, and demonstrates effective performance. Empirical evaluations indicate that the proposed OI-based OOD detector is competitive with state-of-the-art OOD detectors in detection accuracy across a variety of scenarios, while maintaining a more frugal computational and memory footprint. The proposed OI-based confidence score function shows an insensitivity to small distributional shifts and a robustness against Huber ϵ -contamination. Additionally, it shows potential for estimating OI and model accuracy in specific applications. Overall, this paper showcases the effectiveness of using the OI-based metric for OOD detection.

REFERENCES

- [1] H. Fu, P. Krishnamurthy, and F. Khorrami, "Functional replicas of proprietary three-axis attitude sensors via lstm neural networks," in *2020 IEEE Conference on Control Technology and Applications*. IEEE, 2020, pp. 70–75.
- [2] A. Papanicolaou, H. Fu, P. Krishnamurthy, B. Healy, and F. Khorrami, "An optimal control strategy for execution of large stock orders using long short-term memory networks," *Journal of Computational Finance*, vol. 26, no. 4, 2023.
- [3] A. Papanicolaou, H. Fu, P. Krishnamurthy, and F. Khorrami, "A deep neural network algorithm for linear-quadratic portfolio optimization with mgarch and small transaction costs," *IEEE Access*, vol. 11, pp. 16 774–16 792, 2023.
- [4] A. Sarmadi, H. Fu, P. Krishnamurthy, S. Garg, and F. Khorrami, "Privacy-preserving collaborative learning through feature extraction," *IEEE Transactions on Dependable and Secure Computing*, vol. 21, no. 1, pp. 486–498, 2023.
- [5] D. Macêdo, T. I. Ren, C. Zanchettin, A. L. Oliveira, and T. Ludermir, "Entropic out-of-distribution detection: Seamless detection of unknown examples," *IEEE Transactions on Neural Networks and Learning Systems*, vol. 33, no. 6, pp. 2350–2364, 2021.
- [6] Z. Zhao, L. Cao, and K.-Y. Lin, "Out-of-distribution detection by cross-class vicinity distribution of in-distribution data," *IEEE Transactions on Neural Networks and Learning Systems*, 2023.
- [7] C. Wang, J. Jiang, X. Zhou, and X. Liu, "Resmooth: Detecting and utilizing ood samples when training with data augmentation," *IEEE Transactions on Neural Networks and Learning Systems*, 2022.
- [8] H. Fu, N. Patel, P. Krishnamurthy, and F. Khorrami, "Clipscope: Enhancing zero-shot ood detection with bayesian scoring," *arXiv preprint arXiv:2405.14737*, 2024.
- [9] H. Fu, P. Krishnamurthy, and F. Khorrami, "Combining switching mechanism with re-initialization and anomaly detection for resiliency of cyber-physical systems," *Automatica*, vol. 172, p. 111994, 2025.
- [10] B. Schölkopf, J. C. Platt, J. Shawe-Taylor, A. J. Smola, and R. C. Williamson, "Estimating the support of a high-dimensional distribution," *Neural Computation*, vol. 13, no. 7, pp. 1443–1471, 2001.
- [11] L. Ruff, R. Vandermeulen, N. Goernitz, L. Deecke, S. A. Siddiqui, A. Binder, E. Müller, and M. Kloft, "Deep one-class classification," in *Proceedings of International Conference on Machine Learning*, 2018, pp. 4393–4402.
- [12] P. Morteza and Y. Li, "Provable guarantees for understanding out-of-distribution detection," in *Proceedings of the AAAI Conference on Artificial Intelligence*, vol. 8, 2022.
- [13] M. Pastore and A. Calcagni, "Measuring distribution similarities between samples: A distribution-free overlapping index," *Frontiers in Psychology*, vol. 10, p. 1089, 2019.
- [14] Y. Zhang, G. Niu, and M. Sugiyama, "Learning noise transition matrix from only noisy labels via total variation regularization," in *Proceedings of International Conference on Machine Learning*, 2021, pp. 12 501–12 512.
- [15] M. Kapralov, V. Potluru, and D. Woodruff, "How to fake multiply by a gaussian matrix," in *Proceedings of International Conference on Machine Learning*, 2016, pp. 2101–2110.
- [16] "Optimal transport and wasserstein distance," <https://www.stat.cmu.edu/~7elarry=sml/Opt.pdf>, 2019, accessed: 2023-04-09.
- [17] Y. G. Yatracos, "Limitations of the wasserstein mde for univariate data," *Statistics and Computing*, vol. 32, no. 6, p. 95, 2022.
- [18] P. J. Huber, "Robust estimation of a location parameter," *Breakthroughs in Statistics: Methodology and Distribution*, pp. 492–518, 1992.
- [19] D. Hendrycks and K. Gimpel, "A baseline for detecting misclassified and out-of-distribution examples in neural networks," in *Proceedings of International Conference on Learning Representations*, 2017.
- [20] K. Lee, K. Lee, H. Lee, and J. Shin, "A simple unified framework for detecting out-of-distribution samples and adversarial attacks," in *Proceedings of Advances in Neural Information Processing Systems*, vol. 31, 2018, pp. 1–9.
- [21] W. Liu, X. Wang, J. Owens, and Y. Li, "Energy-based out-of-distribution detection," in *Proceedings of Advances in Neural Information Processing Systems*, vol. 33, 2020, pp. 21 464–21 475.
- [22] Y. Zhang, J. Pan, W. Liu, Z. Chen, K. Li, J. Wang, Z. Liu, and H. Wei, "Kullback-leibler divergence-based out-of-distribution detection with flow-based generative models," *IEEE Transactions on Knowledge and Data Engineering*, 2023.
- [23] B. K. Sriperumbudur, K. Fukumizu, A. Gretton, B. Schölkopf, and G. R. Lanckriet, "On the empirical estimation of integral probability metrics," *Electronic Journal of Statistics*, vol. 6, pp. 1550–1599, 2012.
- [24] M. B. Cohen, Y. T. Lee, and Z. Song, "Solving linear programs in the current matrix multiplication time," *Journal of the ACM*, vol. 68, no. 1, pp. 1–39, 2021.
- [25] "Lecture notes 27 36-705," <https://www.stat.cmu.edu/~larry/=stat705/Lecture27.pdf>, 2020, accessed: 2023-01-09.
- [26] F. Schmid and A. Schmidt, "Nonparametric estimation of the coefficient of overlapping—theory and empirical application," *Computational Statistics & Data Analysis*, vol. 50, no. 6, pp. 1583–1596, 2006.
- [27] A. Z. Zambom and D. Ronaldo, "A review of kernel density estimation with applications to econometrics," *International Econometric Review*, vol. 5, no. 1, pp. 20–42, 2013.
- [28] F. D. Comité, F. Denis, R. Gilleron, and F. Letouzey, "Positive and unlabeled examples help learning," in *Proceedings of International Conference on Algorithmic Learning Theory*, 1999, pp. 219–230.
- [29] D. M. J. Tax, "One-class classification: Concept learning in the absence of counter-examples," Ph.D. dissertation, Technische Universiteit Delft, 2002.
- [30] S. S. Khan and M. G. Madden, "One-class classification: taxonomy of study and review of techniques," *The Knowledge Engineering Review*, vol. 29, no. 3, pp. 345–374, 2014.
- [31] P. Perera, R. Nallapati, and B. Xiang, "Ocgan: One-class novelty detection using gans with constrained latent representations," in *Proceedings of the IEEE/CVF Conference on Computer Vision and Pattern Recognition*, 2019, pp. 2898–2906.
- [32] G. Kwon, M. Prabhushankar, D. Temel, and G. AlRegib, "Backpropagated gradient representations for anomaly detection," in *Proceedings of European Conference on Computer Vision*, 2020, pp. 206–226.
- [33] L. Ruff, R. A. Vandermeulen, N. Goernitz, A. Binder, E. Müller, K.-R. Müller, and M. Kloft, "Deep semi-supervised anomaly detection," in *Proceedings of International Conference on Learning Representations*, 2020.
- [34] P. Bergmann, M. Fauser, D. Sattlegger, and C. Steger, "Uninformed students: Student-teacher anomaly detection with discriminative latent embeddings," in *Proceedings of the IEEE/CVF Conference on Computer Vision and Pattern Recognition*, 2020, pp. 4183–4192.
- [35] C.-L. Li, K. Sohn, J. Yoon, and T. Pfister, "Cutpaste: Self-supervised learning for anomaly detection and localization," in *Proceedings of the IEEE/CVF Conference on Computer Vision and Pattern Recognition*, 2021, pp. 9664–9674.
- [36] S. Schneider, D. Antensteiner, D. Soukup, and M. Scheutz, "Autoencoders-a comparative analysis in the realm of anomaly detection," in *Proceedings of the IEEE/CVF Conference on Computer Vision and Pattern Recognition*, 2022, pp. 1986–1992.
- [37] Z. You, K. Yang, W. Luo, L. Cui, Y. Zheng, and X. Le, "Adtr: Anomaly detection transformer with feature reconstruction," in *Proceedings of Neural Information Processing*, 2023, pp. 298–310.
- [38] I. Golan and R. El-Yaniv, "Deep anomaly detection using geometric transformations," in *Proceedings of Advances in Neural Information Processing Systems*, vol. 31, 2018, pp. 1–9.
- [39] C. Qiu, A. Li, M. Kloft, M. Rudolph, and S. Mandt, "Latent outlier exposure for anomaly detection with contaminated data," in *Proceedings of International Conference on Machine Learning*, 2022, pp. 18 153–18 167.
- [40] T. Reiss, N. Cohen, L. Bergman, and Y. Hoshen, "Panda: Adapting pretrained features for anomaly detection and segmentation," in *Pro-*

- ceedings of the IEEE/CVF Conference on Computer Vision and Pattern Recognition*, 2021, pp. 2806–2814.
- [41] M. Salehi, N. Sadjadi, S. Baselizadeh, M. H. Rohban, and H. R. Rabiee, “Multiresolution knowledge distillation for anomaly detection,” in *Proceedings of the IEEE/CVF Conference on Computer Vision and Pattern Recognition*, 2021, pp. 14 902–14 912.
- [42] R. Zhang, P. Isola, A. A. Efros, E. Shechtman, and O. Wang, “The unreasonable effectiveness of deep features as a perceptual metric,” in *Proceedings of the IEEE Conference on Computer Vision and Pattern Recognition*, 2018, pp. 586–595.
- [43] Z. Li, Y. Zhao, X. Hu, N. Botta, C. Ionescu, and G. Chen, “Ecod: Unsupervised outlier detection using empirical cumulative distribution functions,” *IEEE Transactions on Knowledge and Data Engineering*, 2022.
- [44] H. Xu, G. Pang, Y. Wang, and Y. Wang, “Deep isolation forest for anomaly detection,” *IEEE Transactions on Knowledge and Data Engineering*, 2023.
- [45] H. Wang, Z. Li, L. Feng, and W. Zhang, “Vim: Out-of-distribution with virtual-logit matching,” in *Proceedings of the IEEE/CVF Conference on Computer Vision and Pattern Recognition*, 2022, pp. 4921–4930.
- [46] R. Huang, A. Geng, and Y. Li, “On the importance of gradients for detecting distributional shifts in the wild,” in *Proceedings of Advances in Neural Information Processing Systems*, 2021, pp. 677–689.
- [47] X. Du, Z. Wang, M. Cai, and S. Li, “Towards unknown-aware learning with virtual outlier synthesis,” in *Proceedings of International Conference on Learning Representations*, 2022.
- [48] K. Roth, L. Pemula, J. Zepeda, B. Schölkopf, T. Brox, and P. Gehler, “Towards total recall in industrial anomaly detection,” in *Proceedings of the IEEE/CVF Conference on Computer Vision and Pattern Recognition*, 2022, pp. 14 318–14 328.
- [49] A. Zolfi, G. Amit, A. Baras, S. Koda, I. Morikawa, Y. Elovici, and A. Shabtai, “Yolood: Utilizing object detection concepts for multi-label out-of-distribution detection,” in *Proceedings of the IEEE/CVF Conference on Computer Vision and Pattern Recognition*, 2024, pp. 1–8.
- [50] J. Li, P. Chen, Z. He, S. Yu, S. Liu, and J. Jia, “Rethinking out-of-distribution (ood) detection: Masked image modeling is all you need,” in *Proceedings of the IEEE/CVF Conference on Computer Vision and Pattern Recognition*, 2023, pp. 11 578–11 589.
- [51] A. Malinin and M. Gales, “Reverse kl-divergence training of prior networks: Improved uncertainty and adversarial robustness,” in *Proceedings of Advances in Neural Information Processing Systems*, vol. 32, 2019, pp. 1–9.
- [52] E. Even-Dar, S. Mannor, Y. Mansour, and S. Mahadevan, “Action elimination and stopping conditions for the multi-armed bandit and reinforcement learning problems,” *Journal of Machine Learning Research*, vol. 7, no. 6, 2006.
- [53] S. Kolouri, S. R. Park, M. Thorpe, D. Slepcev, and G. K. Rohde, “Optimal mass transport: Signal processing and machine-learning applications,” *IEEE Signal Processing Magazine*, vol. 34, no. 4, pp. 43–59, 2017.
- [54] S. Raghvendra, P. Shirzadian, and K. Zhang, “A new robust partial p -wasserstein-based metric for comparing distributions,” *arXiv preprint arXiv:2405.03664*, 2024.
- [55] A. Phatak, S. Raghvendra, C. Tripathy, and K. Zhang, “Computing all optimal partial transports,” in *International Conference on Learning Representations*, 2023.
- [56] N. Lahn, S. Raghvendra, and K. Zhang, “A combinatorial algorithm for approximating the optimal transport in the parallel and mpc settings,” *Advances in Neural Information Processing Systems*, vol. 36, pp. 21 675–21 686, 2023.
- [57] M. Cuturi and A. Doucet, “Fast computation of wasserstein barycenters,” in *Proceedings of International Conference on Machine Learning*, 2014, pp. 685–693.
- [58] H. F. Inman and E. L. Bradley Jr, “The overlapping coefficient as a measure of agreement between probability distributions and point estimation of the overlap of two normal densities,” *Communications in Statistics-theory and Methods*, vol. 18, no. 10, pp. 3851–3874, 1989.
- [59] T. Gu, K. Liu, B. Dolan-Gavitt, and S. Garg, “Badnets: Evaluating backdooring attacks on deep neural networks,” *IEEE Access*, vol. 7, pp. 47 230–47 244, 2019.
- [60] Y. Liu, S. Ma, Y. Aafer, W.-C. Lee, J. Zhai, W. Wang, and X. Zhang, “Trojaning attack on neural networks,” in *Proceedings of the Network and Distributed Systems Security Symposium*, 2018.
- [61] H. Fu, A. K. Veldanda, P. Krishnamurthy, S. Garg, and F. Khorrami, “A feature-based on-line detector to remove adversarial-backdoors by iterative demarcation,” *IEEE Access*, vol. 10, pp. 5545 – 5558, 2022.
- [62] H. Fu, P. Krishnamurthy, S. Garg, and F. Khorrami, “Differential analysis of triggers and benign features for black-box dnn backdoor detection,” *IEEE Transactions on Information Forensics and Security*, vol. 18, pp. 4668–4680, 2023.
- [63] H. Fu, A. Sarmadi, P. Krishnamurthy, S. Garg, and F. Khorrami, “Mitigating backdoor attacks on deep neural networks,” in *Embedded Machine Learning for Cyber-Physical, IoT, and Edge Computing: Use Cases and Emerging Challenges*. Springer, 2023, pp. 395–431.
- [64] H. Fu, “Enhancing the safety of machine learning systems and cyber-physical systems against cyber attacks,” Ph.D. dissertation, New York University Tandon School of Engineering, 2024.
- [65] B. Biggio, B. Nelson, and P. Laskov, “Poisoning attacks against support vector machines,” in *Proceedings of the International Conference on Machine Learning*, 2012, pp. 1467–1474.
- [66] I. Goodfellow, J. Pouget-Abadie, M. Mirza, B. Xu, D. Warde-Farley, S. Ozair, A. Courville, and Y. Bengio, “Generative adversarial nets,” in *Proceedings of Advances in Neural Information Processing Systems*, vol. 27, 2014, pp. 1–9.
- [67] T. A. Nguyen and A. T. Tran, “Wanet - imperceptible warping-based backdoor attack,” in *Proceedings of the International Conference on Learning Representations*, 2021.
- [68] Y. Li, Y. Li, B. Wu, L. Li, R. He, and S. Lyu, “Invisible backdoor attack with sample-specific triggers,” in *Proceedings of the IEEE/CVF International Conference on Computer Vision*, 2021, pp. 16 463–16 472.
- [69] Y. Zeng, W. Park, Z. M. Mao, and R. Jia, “Rethinking the backdoor attacks’ triggers: A frequency perspective,” in *Proceedings of the IEEE/CVF International Conference on Computer Vision*, 2021, pp. 16 473–16 481.
- [70] Y. Liu, X. Ma, J. Bailey, and F. Lu, “Reflection backdoor: A natural backdoor attack on deep neural networks,” in *Proceedings of European Conference on Computer Vision*, 2020, pp. 182–199.
- [71] B. Wang, Y. Yao, S. Shan, H. Li, B. Viswanath, H. Zheng, and B. Y. Zhao, “Neural cleanse: Identifying and mitigating backdoor attacks in neural networks,” in *Proceedings of IEEE Symposium on Security and Privacy*, 2019, pp. 707–723.
- [72] K. Liu, B. Dolan-Gavitt, and S. Garg, “Fine-pruning: Defending against backdooring attacks on deep neural networks,” in *Proceedings of International Symposium on Research in Attacks, Intrusions, and Defenses*, 2018, pp. 273–294.
- [73] R. Zheng, R. Tang, J. Li, and L. Liu, “Data-free backdoor removal based on channel lipschitzness,” in *Proceedings of the European Conference on Computer Vision*, 2022, pp. 175–191.
- [74] Y. Gao, C. Xu, D. Wang, S. Chen, D. C. Ranasinghe, and S. Nepal, “Strip: A defence against trojan attacks on deep neural networks,” in *Proceedings of the Annual Computer Security Applications Conference*, 2019, pp. 113–125.
- [75] A. K. Veldanda, K. Liu, B. Tan, P. Krishnamurthy, F. Khorrami, R. Karri, B. Dolan-Gavitt, and S. Garg, “Nnoculation: Catching badnets in the wild,” in *Proceedings of the ACM Workshop on Artificial Intelligence and Security*, 2021, pp. 49–60.
- [76] A. Krizhevsky, G. Hinton *et al.*, “Learning multiple layers of features from tiny images,” 2009.
- [77] D. Dua and C. Graff, “UCI machine learning repository,” <http://archive.ics.uci.edu/ml/>, 2017, accessed: 2022-04-09.
- [78] M. Cimpoi, S. Maji, I. Kokkinos, S. Mohamed, and A. Vedaldi, “Describing textures in the wild,” in *Proceedings of the IEEE Conference on Computer Vision and Pattern Recognition*, 2014, pp. 3606–3613.
- [79] Y. Netzer, T. Wang, A. Coates, A. Bissacco, B. Wu, and A. Y. Ng, “Reading digits in natural images with unsupervised feature learning,” in *Proceedings of NIPS Workshop on Deep Learning and Unsupervised Feature Learning*, 2011.
- [80] F. Yu, A. Seff, Y. Zhang, S. Song, T. Funkhouser, and J. Xiao, “Lsun: Construction of a large-scale image dataset using deep learning with humans in the loop,” *arXiv preprint arXiv:1506.03365*, 2015.
- [81] P. Xu, K. A. Ehinger, Y. Zhang, A. Finkelstein, S. R. Kulkarni, and J. Xiao, “Turkergaze: Crowdsourcing saliency with webcam based eye tracking,” *arXiv preprint arXiv:1504.06755*, 2015.
- [82] Y. LeCun, C. Cortes, and C. Burges, “Mnist handwritten digit database,” *ATT Labs [Online]*. Available: <http://yann.lecun.com/exdb/mnist>, vol. 2, 2010.
- [83] J. Stallkamp, M. Schlipsing, J. Salmen, and C. Igel, “The german traffic sign recognition benchmark: A multi-class classification competition,” in *Proceedings of International Joint Conference on Neural Networks*, 2011, pp. 1453–1460.
- [84] L. Wolf, T. Hassner, and I. Maoz, “Face recognition in unconstrained videos with matched background similarity,” in *Proceedings of the IEEE*

Conference on Computer Vision and Pattern Recognition, 2011, pp. 529–534.

- [85] J. Deng, W. Dong, R. Socher, L. Li, Kai Li, and Li Fei-Fei, “Imagenet: A large-scale hierarchical image database,” in *Proceedings of the IEEE Conference on Computer Vision and Pattern Recognition*, 2009, pp. 248–255.
- [86] A. Makhzani and B. J. Frey, “Winner-take-all autoencoders,” in *Proceedings of Advances in Neural Information Processing Systems*, vol. 28, 2015, p. 2791–2799.
- [87] T. Schlegl, P. Seeböck, S. M. Waldstein, U. Schmidt-Erfurth, and G. Langs, “Unsupervised anomaly detection with generative adversarial networks to guide marker discovery,” in *Proceedings of International Conference on Information Processing in Medical Imaging*, 2017, pp. 146–157.
- [88] Y. LeCun, L. Bottou, Y. Bengio, and P. Haffner, “Gradient-based learning applied to document recognition,” *Proceedings of the IEEE*, vol. 86, no. 11, pp. 2278–2324, 1998.
- [89] M. M. Breunig, H.-P. Kriegel, R. T. Ng, and J. Sander, “Lof: identifying density-based local outliers,” in *Proceedings of the ACM SIGMOD International Conference on Management of Data*, 2000, pp. 93–104.
- [90] F. T. Liu, K. M. Ting, and Z.-H. Zhou, “Isolation forest,” in *Proceedings of IEEE International Conference on Data Mining*, 2008, pp. 413–422.
- [91] P. J. Rousseeuw and K. V. Driessen, “A fast algorithm for the minimum covariance determinant estimator,” *Technometrics*, vol. 41, no. 3, pp. 212–223, 1999.
- [92] A. Radford, J. W. Kim, C. Hallacy, A. Ramesh, G. Goh, S. Agarwal, G. Sastry, A. Askell, P. Mishkin, J. Clark *et al.*, “Learning transferable visual models from natural language supervision,” in *Proceedings of International Conference on Machine Learning*, 2021, pp. 8748–8763.
- [93] G. Van Horn, O. Mac Aodha, Y. Song, Y. Cui, C. Sun, A. Shepard, H. Adam, P. Perona, and S. Belongie, “The inaturalist species classification and detection dataset,” in *Proceedings of the IEEE Conference on Computer Vision and Pattern Recognition*, 2018, pp. 8769–8778.
- [94] J. Xiao, J. Hays, K. A. Ehinger, A. Oliva, and A. Torralba, “Sun database: Large-scale scene recognition from abbey to zoo,” in *Proceedings of the IEEE/CVF Conference on Computer Vision and Pattern Recognition*, 2010, pp. 3485–3492.
- [95] B. Zhou, A. Lapedriza, A. Khosla, A. Oliva, and A. Torralba, “Places: A 10 million image database for scene recognition,” *IEEE Transactions on Pattern Analysis and Machine Intelligence*, vol. 40, no. 6, pp. 1452–1464, 2017.
- [96] S. Liang, Y. Li, and R. Srikant, “Enhancing the reliability of out-of-distribution image detection in neural networks,” in *Proceedings of International Conference on Learning Representations*, 2018.
- [97] L. Tao, X. Du, J. Zhu, and Y. Li, “Non-parametric outlier synthesis,” in *Proceedings of The International Conference on Learning Representations*, 2022.
- [98] X. Chen, C. Liu, B. Li, K. Lu, and D. Song, “Targeted backdoor attacks on deep learning systems using data poisoning,” *arXiv preprint arXiv:1712.05526*, 2017.
- [99] Y. Liu, W.-C. Lee, G. Tao, S. Ma, Y. Aafer, and X. Zhang, “Abs: Scanning neural networks for back-doors by artificial brain stimulation,” in *Proceedings of the 2019 ACM SIGSAC Conference on Computer and Communications Security*, 2019, pp. 1265–1282.
- [100] L. Zhang, M. Goldstein, and R. Ranganath, “Understanding failures in out-of-distribution detection with deep generative models,” in *Proceedings of International Conference on Machine Learning*, 2021, pp. 12427–12436.

APPENDIX

A. Proof of Theorem III.3

Definition A.1 (Total Variation Distance (TVD)). TVD $\delta : \mathbb{R}^n \times \mathbb{R}^n \rightarrow [0, 1]$ of P and Q is defined as:

$$\delta(P, Q) = \frac{1}{2} \int_{\mathbb{R}^n} |f_P(x) - f_Q(x)| dx. \quad (11)$$

Since $\text{OI} + \text{TVD} = 1$, we have $\eta = 1 - \delta = 1 - \delta_A - \delta_{\mathbb{R}^n \setminus A}$.

Proof. Let f_{D^+} and f_{D^-} be the probability density functions for D^+ and D^- . From **Definition A.1**, we have

$$\eta(D^+, D^-) = 1 - \delta_A(D^+, D^-) - \delta_{A^c}(D^+, D^-). \quad (12)$$

Using (12), triangular inequality, and boundedness, we obtain

$$\|\mu_{D^+} - \mu_{D^-}\| = \left\| \int_B x (f_{D^+}(x) - f_{D^-}(x)) dx \right\| \quad (13)$$

$$\leq \int_B \|x\| |f_{D^+}(x) - f_{D^-}(x)| dx \quad (14)$$

$$= \int_A \|x\| \cdot |f_{D^+}(x) - f_{D^-}(x)| dx \quad (15)$$

$$+ \int_{A^c} \|x\| \cdot |f_{D^+}(x) - f_{D^-}(x)| dx \quad (16)$$

$$\leq 2r_A \delta_A + 2r_{A^c} \delta_{A^c} \quad (17)$$

$$= 2r_A \delta_A + 2r_{A^c} (1 - \delta_A - \eta(D^+, D^-)) \quad (18)$$

which implies (3). Since $1 - \delta_A - \eta(D^+, D^-) \geq 0$, we can replace r_{A^c} with r_B in (18) to get (4). \square

B. Proof of Corollary III.4

Proof. Let $g : B \rightarrow \{0, 1\}$ be a condition function and define $A(g) = \{x \mid g(x) = 1, x \in B\}$. According to the definition of δ_A and triangular inequality, we have

$$\delta_{A(g)}(D^+, D^-) = \frac{1}{2} \int_{A(g)} |f_{D^+}(x) - f_{D^-}(x)| dx \quad (19)$$

$$\geq \frac{1}{2} \left| \int_{A(g)} f_{D^+}(x) - f_{D^-}(x) dx \right| \quad (20)$$

$$= \frac{1}{2} \left| \int_{\mathbb{R}^n} g(x) f_{D^+}(x) - g(x) f_{D^-}(x) dx \right|$$

$$= \frac{1}{2} |\mathbb{E}_{D^+}[g] - \mathbb{E}_{D^-}[g]|. \quad (21)$$

Applying (21) into **Theorem III.3** gives **Corollary III.4**. \square

C. Proof of Proposition V.1

Proof. Since the support is $[0, 1]$, we have $r_B = 1$, $\mu_{D^+} - \mu_{D^-} = -\int_0^1 x \sin 2\pi\omega x dx \leq \frac{1}{\omega}$, $\mathbb{E}_{D^+}[g] - \mathbb{E}_{D^-}[g] = -\int_0^1 g(x) \sin 2\pi\omega x dx \leq \frac{1}{\omega}$, and $\bar{\eta} \geq 1 - \frac{1}{2\omega} - \max_g \frac{1-r_{A(g)}}{2} \frac{1}{\omega} \geq 1 - \frac{1}{\omega}$. \square

D. Proof of Proposition V.2

Proof. Denote $Q = (1 - \epsilon)D^+ + \epsilon D^-$, then $\mu_{D^+} - \mu_Q = \epsilon(\mu_{D^+} - \mu_{D^-})$, $\mathbb{E}_{D^+}[g] - \mathbb{E}_Q[g] = \epsilon(\mathbb{E}_{D^+}[g] - \mathbb{E}_{D^-}[g])$, and $\bar{\eta}(D^+, Q) = 1 - \epsilon(\frac{1}{2r_B} \|\mu_{D^+} - \mu_{D^-}\| + \max_g \frac{r_B - r_{A(g)}}{2r_B} |\mathbb{E}_{D^+}[g] - \mathbb{E}_{D^-}[g]|) \geq 1 - \epsilon$. \square

E. Proof of Theorem V.3

Proof. Let f_D and f_{D^*} be their probability density functions, $\text{Acc} = \int_{x \sim D^*} \left(p \frac{\min\{f_D(x), f_{D^*}(x)\}}{f_{D^*}(x)} + q \left(1 - \frac{\min\{f_D(x), f_{D^*}(x)\}}{f_{D^*}(x)} \right) \right) \times f_{D^*}(x) dx = p\eta(D, D^*) + q(1 - \eta(D, D^*)) \leq (p - q)(1 - \frac{1}{2r_B} \|\mu_D - \mu_{D^*}\| - \max_g \frac{r_B - r_{A(g)}}{2r_B} |\mathbb{E}_D[g] - \mathbb{E}_{D^*}[g]|) + q$. \square

F. Details for Fig. 2

The numerical results are given in Table X.

TABLE X
AUROC (%) FOR DIFFERENT METHODS ON UCI DATASETS.

| | | | |
|---------------------------|-----------------------------|--------------------------------|----------------------|
| Ours | L1-Ball | K-Center | Parzen |
| 97.67 ± 2.55 | 90.19 ± 22.21 | 92.4 ± 10.24 | 93.99 ± 9.92 |
| Gaussian | K-Mean | 1-Nearest Neighbor | K-Nearest Neighbor |
| 95.83 ± 6.45 | 94.51 ± 5.7 | 93.24 ± 11.05 | 93.24 ± 11.05 |
| Auto-Encoder Network | Linear Programming | Principal Component | Lof Range |
| 87.81 ± 22.15 | 81.5 ± 34.42 | 81.8 ± 25.18 | 86.04 ± 23.54 |
| Nearest Neighbor Distance | Minimum Spanning Tree | Minimum Covariance Determinant | Self Organizing Map |
| 84.54 ± 15.91 | 92.32 ± 11.4 | 94.1 ± 11.56 | 93.6 ± 7.49 |
| Support Vector Machine | Minimax Probability Machine | Mixture Gaussians | Local Outlier Factor |
| 78.69 ± 36.72 | 77.84 ± 35.57 | 93.61 ± 11.15 | 89.04 ± 13.77 |
| Naive Parzen | Local Correlation Integral | | |
| 97.41 ± 2.59 | 96.79 ± 2.45 | | |

| Clean | Triggers | | | Clean | Triggers |
|----------|-----------|---------|---------|--------------|------------|
| MNIST | All label | Naive.1 | Naive.2 | ImageNet | Invisible |
| | | | | | |
| CIFAR-10 | TCA.1 | TCA.2 | Wanet | YouTube Face | Sunglasses |
| | | | | | |
| GTSRB | Moving | Filter | Wanet | | Lipstick |
| | | | | | |

Fig. 7. Pictures under “Triggers” are poisoned samples. Pictures under “Clean” are clean samples.

G. Backdoor Detection

The datasets are balanced by having an equal number of clean and poisoned samples. For each backdoor attack, we assume that a small clean validation dataset is available (i.e., ten samples from each class) at the beginning. Therefore, the poisoned samples (i.e., samples attached with triggers) can be considered OOD, whereas the clean samples can be considered ID. The metrics used are: TPR95 (i.e., the detection accuracy for poisoned samples when the detection accuracy for clean samples is 95%), AUROC, and AUPR. We have carefully finetuned the baseline methods’ hyperparameters to ensure their best performance over other hyperparameter choices. Fig. 7 shows the utilized triggers, and Table XI shows the details for backdoor detection. For most triggers, our method has over 96% of TPR95, over 97% of AUROC, and 95% of AUPR. Our detector is robust against the latest or advanced backdoor attacks, such as Wanet, invisible trigger, all label attack, and filter attack, whereas the baseline methods show low performance on those attacks. The Gaussian-based baseline methods encountered an error for two cases because the data features are dependent.

H. Experimental Illustration of Theorem V.3

Setup: We use MNIST, GTSRB, YouTube Face, and sub-ImageNet and their domain-shifted versions given in Fig. 8 to illustrate the theorem. We set $\sigma = 0, 0.1, \dots, 0.9, 1$ and calculated the RHS of (10) using $L_1, L_2,$ and L_∞ norms in the raw image input space, model output space, and hidden layer space. We use $g_j(x) = \mathbb{1}\{|x| \leq r_j\}$. Fig. 9 shows the model accuracy and corresponding upper bounds with different norms and σ s. The model accuracy is below all calculated upper limits, validating the theorem. The difference between model accuracy and the calculated upper bound accuracy can reflect the extent of the domain shift in the test dataset. From Fig. 9, a large difference reflects a large domain shift. When the domain shift vanishes, the model accuracy and the calculated upper bound accuracy are close.

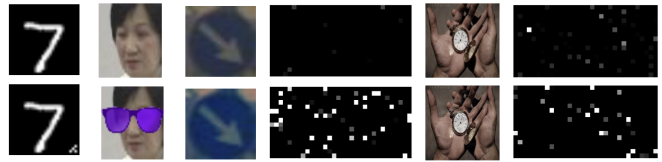


Fig. 8. Top: original samples. Bottom: domain-shifted samples. From left to right: MNIST, YouTube Face, GTSRB, GTSRB in hidden layer space, ImageNet, ImageNet in hidden layer space.

From Fig. 9, the calculated upper bound accuracy varies with spaces. The inference is that a low calculated upper bound accuracy implies a high likelihood of detecting domain-shifted data in that particular utilized space. For example, in Fig. 9 MNIST and YouTube, the input space with L_∞ norm shows the lowest upper bound accuracy. Therefore, domain-shifted samples will likely be detected in the input space. Indeed, from Fig. 8, even vision inspection can easily detect them. As for GTSRB and ImageNet, the input space has the highest upper limit lines. Therefore, domain-shifted samples are less likely to be detected in the input space. Fig. 8 shows that the visual inspection can barely detect them. However, the hidden

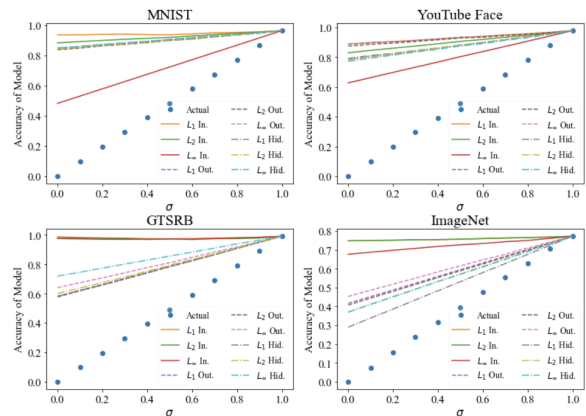


Fig. 9. The model accuracy vs. (10) calculated with $L_{1,2,\infty}$ norms in input, output, and hidden spaces. X-axis is the ratio of clean samples to the entire testing samples.

TABLE XI
COMPARISON RESULTS FOR BACKDOOR DETECTION (HIGHER NUMBER IMPLIES HIGHER ACCURACY).

| Datasets | Trigger | Metrics (%) | Ours | STRIP | Mahalanobis | GEM | MSP |
|---------------------|------------|-------------|--------------|--------------|-------------------------------|--------------|------------|
| MNIST | All label | TPR95 | 83.05 | 2.58 | 50.83 | 100 | 100 |
| | | AUROC | 96.13 | 44.69 | 90.78 | 50.43 | 50 |
| | | AUPR | 94.20 | 35.47 | 86.71 | 70.94 | 70.83 |
| MNIST | Naive.1 | TPR95 | 100 | 98.85 | 99.86 | 100 | 5.11 |
| | | AUROC | 97.50 | 97.32 | 97.49 | 53.95 | 51.64 |
| | | AUPR | 96.17 | 95.95 | 96.38 | 74.74 | 50.41 |
| MNIST | Naive.2 | TPR95 | 96.53 | 67.46 | 35.16 | 100 | 14.69 |
| | | AUROC | 97.28 | 93.67 | 78.63 | 53.51 | 58.14 |
| | | AUPR | 95.75 | 89.85 | 78.65 | 74.62 | 64.16 |
| CIFAR-10 | TCA.1 | TPR95 | 100 | 35.68 | 100 | 100 | 4.38 |
| | | AUROC | 97.50 | 83.00 | 97.49 | 50 | 49.23 |
| | | AUPR | 95.47 | 73.22 | 97.84 | 76.32 | 52.64 |
| CIFAR-10 | TCA.2 | TPR95 | 100 | 27.86 | 100 | 100 | 0.02 |
| | | AUROC | 97.50 | 68.79 | 97.49 | 50 | 29.90 |
| | | AUPR | 97.63 | 72.41 | 95.86 | 67.86 | 18.05 |
| CIFAR-10 | Wanet | TPR95 | 37.87 | 0.07 | 20.35 | 22.90 | 100 |
| | | AUROC | 92.74 | 34.97 | 50.61 | 57.81 | 50 |
| | | AUPR | 89.95 | 37.42 | 57.30 | 68.48 | 74.87 |
| GTSRB | Moving | TPR95 | 99.99 | 54 | | | |
| | | AUROC | 85.39 | 7.29 | Fail: dependent data features | | |
| | | AUPR | 96.96 | 89.07 | | | |
| GTSRB | Filter | TPR95 | 85.39 | 7.29 | | | |
| | | AUROC | 96.54 | 38.92 | Fail: dependent data features | | |
| | | AUPR | 95.42 | 38.81 | | | |
| GTSRB | Wanet | TPR95 | 100 | 1.24 | 0.51 | 100 | 100 |
| | | AUROC | 97.50 | 36.31 | 54.46 | 50 | 50 |
| | | AUPR | 97.62 | 39.53 | 48.92 | 75.23 | 75.23 |
| YouTube Face | Sunglasses | TPR95 | 73.37 | 83.03 | 71.64 | 98.58 | 13.06 |
| | | AUROC | 95.21 | 94.80 | 94.38 | 84.29 | 66.55 |
| | | AUPR | 93.00 | 95.54 | 94.63 | 88.83 | 53.27 |
| YouTube Face | Lipstick | TPR95 | 96.64 | 90.14 | 90.88 | 94.18 | 3.73 |
| | | AUROC | 97.21 | 93.15 | 93.26 | 80.80 | 50.14 |
| | | AUPR | 96.30 | 94.98 | 95.09 | 86.53 | 53.27 |
| sub-ImageNet | Invisible | TPR95 | 100 | 7.01 | 0.5 | 100 | 51.40 |
| | | AUROC | 97.49 | 66.26 | 4.78 | 50 | 93.61 |
| | | AUPR | 96.53 | 62.83 | 12.27 | 75.26 | 92.46 |
| Average Performance | | TPR95 | 89.40 | 39.60 | 56.97 | 91.57 | 39.24 |
| | | AUROC | 96.68 | 70.30 | 75.94 | 58.08 | 54.92 |
| | | AUPR | 95.42 | 68.76 | 76.37 | 75.88 | 60.52 |

layer space gives the lowest upper bound accuracy. Therefore, domain-shifted samples are more likely to be distinguished in the hidden layer space, as shown in Fig. 8. The AUROC is 96.54% for GTSRB and 97.49% for ImageNet according to Table XI.